Midlatitude Atmosphere–Ocean Interaction during El Niño. Part II: The Northern Hemisphere Atmosphere

MICHAEL A. ALEXANDER

Department of Meteorology and Center for Climatic Research, University of Wisconsin—Madison, Madison, Wisconsin

(Manuscript received 3 May 1991, in final form 2 January 1992)

ABSTRACT

The influence of midlatitude air–sea interaction on the atmospheric anomalies associated with El Niño is investigated by coupling the Community Climate Model to a mixed-layer ocean model in the North Pacific. Prescribed El Niño conditions, warm sea surface temperatures (SST) in the tropical Pacific, cause a southward displacement and strengthening of the Aleutian Low. This results in enhanced (reduced) advection of cold Asian air over the west-central (northwest) Pacific and northward advection of warm air over the eastern Pacific. Allowing air–sea feedback in the North Pacific slightly modified the El Niño–induced near-surface wind, air temperature, and precipitation anomalies. The anomalous cyclonic circulation over the North Pacific is more concentric and shifted slightly to the east in the coupled simulations. Air–sea feedback also damped the air temperature anomalies over most of the North Pacific and reduced the precipitation rate above the cold SST anomaly that develops in the central Pacific.

The simulated North Pacific SST anomalies and the resulting Northern Hemisphere atmospheric anomalies are roughly one-third as large as those related to the prescribed El Niño conditions in a composite of five cases. The composite geopotential height anomalies associated with changes in the North Pacific SSTs have an equivalent barotropic structure and range from −65 m to 50 m at the 200-mb level. Including air–sea feedback in the North Pacific tended to damp the atmospheric anomalies caused by the prescribed El Niño conditions in the tropical Pacific. As a result, the zonally elongated geopotential height anomalies over the West Pacific are reduced and shifted to the east. However, the atmospheric changes associated with the North Pacific SST anomalies vary widely among the five cases.

1. Introduction

During El Niño events when warm sea surface temperature (SST) anomalies spread across the equatorial Pacific, SST anomalies also develop in the North Pacific. The extratropical anomaly pattern often features cold water in the central Pacific and warm water along the coast of North America. Using atmosphere–ocean model simulations, Alexander (1990a, referred to as MAA; and 1992, Part I of this study) has shown that changes in the atmospheric circulation associated with El Niño can cause realistic SST anomalies to form in the North Pacific Ocean. In Part II of this study we examine how air–sea feedback in the North Pacific influences the atmospheric response to prescribed El Niño conditions in the tropical Pacific.

The effect of SST anomalies on the atmospheric circulation has been widely studied over the past 30 years. Observational analyses by Namias (e.g., 1959, 1965, 1969, 1972), Bjerknes (1964), and Ratcliffe and Murray (1970) have indicated that midlatitude SST anomalies influence the atmospheric circulation both in the vicinity and downstream of the SST anomaly. Motivated by these analyses, Spar (1973), Houghton et al. (1974), Chervin et al. (1976), Kutzbach et al. (1977), Shukla and Bangaru (1979), and Chervin et al. (1980) investigated the response to prescribed SST anomalies in atmospheric models. While the SST anomalies caused changes in the model fields, the signal-to-noise ratio was low unless unrealistically large SST anomalies were prescribed.

Salmon and Hendershott (1976), using a two-level atmospheric model coupled to a 10-m slab ocean, found that the atmosphere appeared to cause anomalies to form in the ocean, rather than the reverse. This result was confirmed by the data analyses of Davis (1976) and Haworth (1978), which indicated that sea level pressure (SLP) anomalies led SST anomalies by one month. The prediction of SLP and surface air temperature from previous SST anomalies was somewhat more encouraging when stratified by season (Davis 1978; Harnack 1979, 1982; Walsh and Richman 1981). However, the amount of explained variance was small (<20%), and the correlation between anomalies in the midlatitude SST and SLP may result from both being affected by conditions in the tropical Pacific (Frankignoul 1985b; MAA; Part I).

Corresponding author address: Dr. Michael A. Alexander, University of Colorado, CIRES, Campus Box 449, Boulder, CO 80309-0449.

© 1992 American Meteorological Society

In contrast to the midlatitude results, observations, dynamical studies, and general circulation model (GCM) simulations in the early 1980s indicated that tropical SST anomalies had a significant impact on both the tropical and midlatitude atmosphere. Horel and Wallace (1981), van Loon and Madden (1981), Pan and Oort (1983), and others found statistical evidence linking the tropical SST anomalies with many atmospheric quantities, including a series of geopotential height anomalies that closely resembled the Pacific/North American (PNA) pattern (Wallace and Gutzler 1981). Many of the atmospheric anomalies observed during El Niño were reproduced in GCM experiments (e.g., Keshevamurty 1982; Blackmon et al. 1983; Shukla and Wallace 1983). Anomalies similar to the PNA pattern found in simple dynamical models (Hoskins and Karoly 1981; Webster 1981), were attributed to the dispersion of Rossby waves on a sphere. However, Geisler et al. (1985) and Wallace and Jiang (1987) found that linear Rossby wave theory could not explain several aspects of the atmospheric changes associated with El Niño. For example, when enhanced convection, a Rossby wave source, moves to different locations in the tropical Pacific, the PNA pattern remains fixed. The dynamical link between the tropical and extratropical anomalies, while still unclear, has been the focus of several recent investigations (Simmons et al. 1983; Kang and Lau 1986; Sardeshmukh and Hoskins 1988; Webster and Chang 1988).

Studies conducted during the last decade using improved models and more complete datasets suggest that the response of the extratropical atmospheric to midlatitude SST anomalies may not be negligible. Hendon and Hartmann (1982) investigated the response of a steady-state, primitive equation model to imposed diabatic heat sources. The linear wave response to shallow thermal forcing was moderately strong when the source was placed in midlatitudes. When feedback between the anomalous atmospheric circulation and surface temperature was included, it enhanced the response to the midlatitude forcing but strongly damped the model's response to subtropical forcing. In a series of studies, Hannoschöck and Frankignoul (1985), Frankignoul (1985a), and Frankignoul and Molin (1988a,b) detected a statistically significant atmospheric response to SST anomalies in the North Pacific in the Goddard Institute for Space Science (GISS) GCM. However, the response was weak and changed substantially when a slightly improved version of the GCM was employed. Palmer and Sun (1985) forced the U.K. Meteorological Office GCM with large (±4°C) warm and cold anomalies off the Newfoundland coast and found a substantial downstream atmospheric response. They also performed an observational analysis which indicated that the SST anomalies originally formed as a result of changes in the atmospheric circulation.

The relative impact of tropical and midlatitude SST anomalies on atmospheric variability was recently studied by Wallace and Jiang (1987) and Lau and Nath (1990). Wallace and Jiang found that the observed midlatitude atmospheric anomalies were better correlated with midlatitude rather than with tropical SST anomalies, but again, the maximum correlations occurred when the atmosphere led the ocean. In addition, the geopotential height anomalies associated with midlatitude SSTs resembled the PNA and the west Atlantic (WA) teleconnection patterns, while the anomalies associated with tropical SST covered large zonal bands. Lau and Nath used the observed monthly varying SST field for the period of 1950–79 as the boundary conditions for a 30-year Geophysical Fluid Dynamics Lab (GFDL) GCM integration. The major atmospheric teleconnection patterns simulated by the model were strongly tied to specific regions in the midlatitude oceans and only weakly correlated with tropical SST anomalies, in agreement with Wallace and Jiang's results.

The modeling study of Pitcher et al. (1988) is particularly relevant to our experiments as both studies have investigated the response of the same GCM to realistic midlatitude and tropical SST anomalies. Pitcher et al. diagnosed the response of the National Center for Atmospheric Research (NCAR) Community Climate Model (CCM) to the observed SST anomaly field in the North Pacific during the winter of 1976/77, which included some of the largest SST anomalies on record. As in most other recent GCM experiments (e.g., Palmer and Sun 1985; Frankignoul 1985a), equivalent barotropic height anomalies formed downstream of the midlatitude SST anomaly. The CCM response to the specified SST anomalies was statistically significant and resembled the PNA pattern. In an additional simulation, the SST anomalies in the North Pacific were combined with a warm anomaly in the tropical Pacific, resulting in an SST pattern that often occurs during El Niño. The CCM response to the combined midlatitude/tropical SST anomaly approximately equaled the sum of the model's response to the individual SST anomalies.

In the modeling studies discussed previously (except Salmon and Henderschott 1976), the ocean temperatures were prescribed, yet the data analyses strongly indicate that midlatitude SST anomalies usually form in response to changes in the atmospheric circulation. In addition, most of the modeling studies specified large SST anomalies that were fixed in time and space. The atmospheric anomalies that develop in a fully interactive system may be quite different from the anomalies that form when SSTs are prescribed. Clearly, using coupled atmosphere–ocean models will facilitate our ability to understand the relationship between midlatitude SST anomalies and the atmospheric circulation.

In this study, a series of CCM–North Pacific Ocean model experiments (section 2) are used to examine how midlatitude air–sea interaction influences the atmospheric response to prescribed El Niño conditions

in the tropical Pacific. The atmospheric response to the tropical SST anomalies is briefly discussed in section 3. The relationships between surface energy fluxes, near-surface atmospheric fields, and air–sea feedback over the North Pacific are examined in section 4. The effects of the developing extratropical SST anomalies on the atmosphere, discussed in section 5, are assessed by comparing coupled CCM–North Pacific Ocean model simulations to CCM simulations in which climatological SSTs are prescribed in the North Pacific. The results are summarized and discussed in section 6.

2. Experiment design

A detailed description of the ocean configuration, the ocean model, and the model simulations is given in Part I; aspects of the experiment design relevant to the atmospheric anomalies associated with midlatitude and tropical SSTs are presented here.

a. The atmosphere and ocean models

The CCM (version 0A) is a 9-layer, sigma-coordinate, primitive equation GCM (for a detailed description see Washington 1982). The model uses spherical harmonics as horizontal basis functions with rhomboidal truncation at wavenumber 15, corresponding to a horizontal resolution of approximately 4.45° latitude by 7.5° longitude. Physical processes include interactive clouds and radiative processes (Ramanathan et al. 1983). Sea ice, snow cover, and the surface hydrology are prescribed. The fidelity of the model under perpetual January and July conditions is discussed by Pitcher et al. (1983) and Malone et al. (1984); the seasonal cycle version, used in this study, is described by Chervin (1986).

The ocean model, located between 20°N and 60°N in the North Pacific, consists of a grid of independent-column models. Vertical processes including surface energy fluxes, penetrating solar radiation, entrainment, and Ekman pumping are represented in each column, but there is no horizontal communication between columns. The column models, which are collocated with the CCM grid points, consist of a bulk mixed-layer model connected to a simple convective–diffusive model. The equations used to compute the temperature, salinity, and mixed-layer depth and the local wind-driven currents are from Niiler and Kraus (1977) and Pollard and Millard (1970), respectively. The convective–diffusive model simulates temperature for three upper layers of the ocean that are 40, 80, and 120 m thick. The temperature beneath the mixed layer is obtained using empirical formulas derived from Heald and Kim (1979) that act to conserve heat between the mixed-layer and convective–diffusive models. Semtner (1984) employed a similar ocean model coupled to a simple atmospheric model to examine climate variability.

b. Model simulations

The experiment utilizes three sets of CCM simulations: uncoupled climate (UNCL), uncoupled El Niño (UNEL), and coupled El Niño (COEL). Climatological SSTs are prescribed at all ocean grid points in the UNCL simulations.[1] The prescribed SST field in the UNEL simulations includes idealized El Niño SSTs in the tropical Pacific and climatological SSTs at all other ocean grid points. In the COEL simulations, the CCM is coupled to a mixed-layer ocean model in the North Pacific; the prescribed SSTs outside the model domain are identical to those in the UNEL set, which are El Niño conditions in the tropical Pacific and climatological SSTs at the remaining ocean grid points.

The sea-ice distribution and climatological SSTs, obtained from the analysis of Alexander and Mobley (1976), are updated daily and have the identical seasonal cycle in all of the simulations. In the UNEL and COEL simulations prescribed tropical SST anomalies are added to the climatological field between 20°N and 30°S in the Pacific. The SST anomalies in the tropical Pacific, which have the same evolution in all of the UNEL and COEL simulations, are derived from the El Niño composite of Rasmusson and Carpenter (1982). Following Aragão (1986), a cubic spline is used to interpolate the three-month average SST anomalies from the composite to daily anomaly values. The anomalies are then doubled in order to obtain ocean temperatures that are more representative of a single strong El Niño episode and to ensure a reasonably strong atmospheric response (Blackmon et al. 1983; Aragão 1986). During the transition and mature phases of El Niño, which occur during boreal fall and winter, positive SST anomalies cover most of the tropical Pacific.

Each CCM experiment set (UNCL, UNEL, COEL) consists of five simulations; the simulations are all nine months in duration and extend from June through the following February. The initial atmospheric fields are selected from five different years of a 20-year seasonal cycle simulation described by Chervin (1986). The same fields are used to initialize the corresponding run within each set; for example, the first simulation in the UNCL, UNEL, and COEL sets are started with identical atmospheric values. The same initial conditions are used in the North Pacific Ocean model in all five COEL integrations. The initial ocean state, a six-year average of conditions on 1 June, is obtained from an extended ocean model integration driven by CCM surface fields.

[1] COCL simulations in which the CCM is coupled to the North Pacific Ocean model and climatological SSTs are prescribed at all other ocean grid points have also been performed. The COCL fields are generally similar to those in the UNCL set over most of the Northern Hemisphere; differences between the sets are most notable in the vicinity of Siberia.

TABLE 1. The SST anomaly location and the associated atmospheric anomalies obtained from the difference between the three sets of simulations. UNCL, UNEL, and COEL are the uncoupled climate, uncoupled El Niño, and coupled El Niño simulations, respectively. The identifiers TP and NP refer to the SST anomalies in the tropical Pacific and North Pacific and the associated atmospheric anomalies. The atmospheric anomalies are examined over the Northern Hemisphere.

Difference	SST anomaly location/ method of obtaining anomalies	Identifier	Location of atmospheric analysis
UNEL-UNCL	Tropical Pacific (prescribed)	TP	Northern Hemisphere
COEL-UNEL	North Pacific (simulated)	NP	Northern Hemisphere
COEL-UNCL	Tropical/North Pacific (prescribed/simulated)	TP/NP	Northern Hemisphere

Regional SST anomalies and the associated atmospheric anomalies are obtained from the difference between the ensemble average of each of the three sets (Table 1). Atmospheric anomalies are associated with the SST anomalies in the tropical Pacific (TP = UNEL − UNCL), the North Pacific (NP = COEL − UNEL), and in both the tropical and North Pacific (TP/NP = COEL − UNCL). The prescribed TP and the ensemble average of the five simulated NP SST anomaly fields during winter are shown in Fig. 1. Model fields are presented for December–January–February (DJF), when the influence of SST anomalies on the extratropical atmosphere is strongest (Walsh and Richman 1981; Wallace and Jiang 1987; Lau and Nath 1990). Following Chervin and Schneider (1976), the pooled t statistic is used to assess the statistical significance of the difference between the model sets. In this experiment, which has 8 degrees of freedom, the 5% significance level corresponds to a two-sided t-statistic value of 2.31.

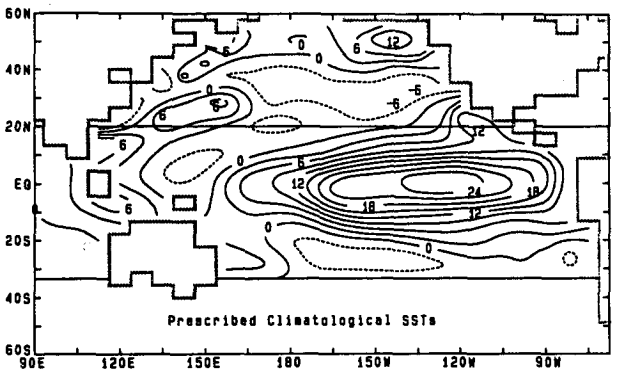

FIG. 1. The prescribed tropical Pacific (TP) SST anomaly field (30°S to 20°N) and simulated North Pacific (NP) SST anomaly field (20°N to 60°N) for the three-month period of December through February. The contour interval is 0.3°C × 10. The tropical anomaly is obtained by doubling the Rasmusson and Carpenter (1982) composite of the SST anomaly pattern during El Niño. The midlatitude anomaly is obtained from the difference between prescribed climatological SSTs and the North Pacific ocean model temperature, as part of the NP experiment. (Note that the North Pacific anomalies shown here are slightly different from those in Fig. 12 of Part I where the climatological SSTs were obtained from ocean model simulations.) The values at grid points located at 20°N are computed by the ocean model; the predicted anomalies were not forced to match the prescribed anomalies at the edge of the model domain.

The results, discussed in the following sections, are likely to be influenced by the limitations of the models. The ocean model used in this study does not include advection, which may be important in generating and maintaining midlatitude SST anomalies. As discussed in MAA and Part I, a large correction of the atmosphere-to-ocean fluxes is required to obtain realistic climatological SSTs in the ocean model. The simulated climatology and the formation of anomalies in the atmosphere are likely to be sensitive to the physical parameterizations used in CCM0A. For example, the large-scale diabatic heating in the CCM0B (which has the same model physics as CCM0A) is generally weaker and confined closer to the surface than in CCM1 (Hoerling et al. 1990). This could have a substantial effect on the mean long-wave pattern and the evolution of circulation anomalies. Errors in the CCM0A surface fluxes and vertical transport of heat and moisture result from the limited vertical resolution and the crude parameterization of boundary-layer processes. In general, storms in the CCM are weak due in part to the coarse horizontal resolution.

3. Atmospheric anomalies associated with tropical Pacific SSTs

The Northern Hemisphere response to prescribed tropical Pacific (TP) SST anomalies is briefly described and compared with observations and other CCM studies. The results are subsequently used to examine changes in the surface fluxes and low-level atmospheric fields over the North Pacific during El Niño and to compare the TP anomalies with those that result from air–sea interaction in the North Pacific.

The ensemble TP SLP and the 700-mb and 200-mb geopotential height anomalies are shown in Fig. 2. The large negative SLP anomaly in the central North Pacific suggests that during El Niño the Aleutian Low deepens and is displaced southeastward from its climatological position, in agreement with observations (Bjerknes 1969; Namias 1976). Positive SLP anomalies are found throughout the high latitudes with a maximum north of Siberia. The midlatitude anomaly pattern has an

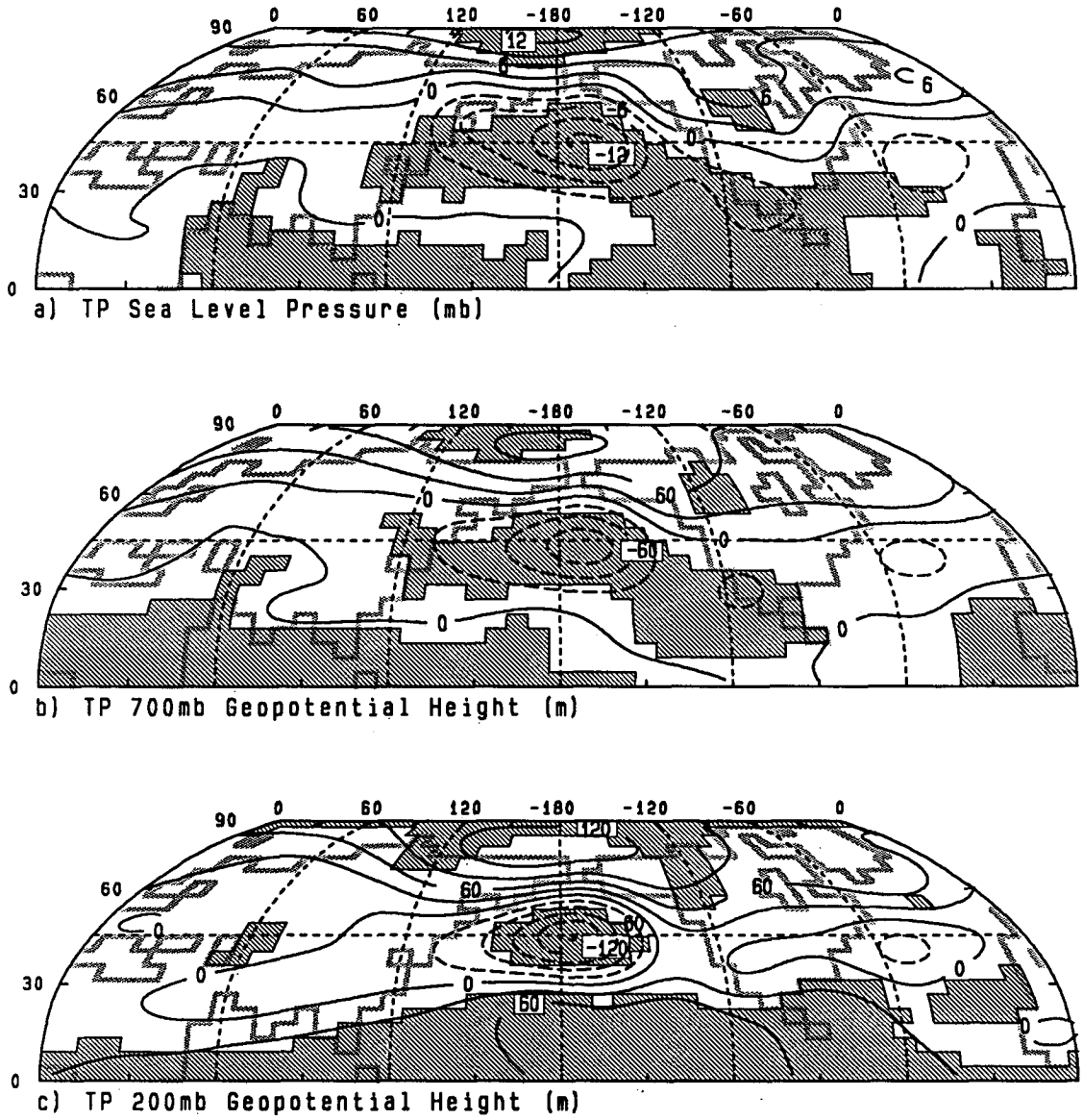

FIG. 2. The winter (December–January–February) TP anomaly fields of (a) SLP, (b) 700-mb height, and (c) 200-mb height. The contour interval is 3 mb in (a), and 30 m in (b) and (c). Grid squares where the t statistic is significant at the 5% level are shaded.

equivalent barotropic structure, and the anomalies increase with height, as found in previous studies. The upper-level TP anomaly fields contain zonal bands with negative anomalies between 30°N and 60°N and positive anomalies north of 60°N. Within these bands anomaly maxima are located between ~140°E and 140°W and to a lesser extent between 20°W and 70°W. These anomaly centers closely resemble the west Pacific (WP) and west Atlantic (WA) teleconnection patterns (Wallace and Gutzler 1981) and the observed correlations between geopotential height and tropical SSTs (Wallace and Jiang 1987). As noted by Wallace and Jiang, the atmospheric anomalies associated with tropical SSTs differ from the PNA pattern in that the anomalies have a more zonal structure and the maximum amplitudes are located farther to the west in the Pacific sector.

The TP SLP and geopotential height anomalies are significant at the 5% level, as indicated by the shaded grid squares, over the central North Pacific, the Arctic Ocean, and northern Canada (Fig. 2). The small but statistically significant SLP anomalies in the tropical Pacific associated with the Southern Oscillation and the positive height anomalies throughout the tropics have been well documented in previous studies.

The positions of the anomalies in Fig. 2 are broadly

similar to those in the experiments of Blackmon et al. (1983) and Aragão (1986), who examined the impact of comparable tropical SST anomalies on the CCM0A. The atmospheric anomalies in our experiment are generally smaller than those in the perpetual January simulations of Blackmon et al. but are substantially larger than those reported by Aragão. The observed anomalies (van Loon and Madden 1981; van Loon and Rogers 1981) are somewhat smaller than ours and slightly larger than those found by Aragão. Our uncoupled El Niño simulations are reintegrations of those used by Aragão, with the addition of a mass conservation scheme in the CCM and the removal of small prescribed SSTs between 20°N and 30°N. The development of sizeable differences between the two sets of simulations indicates the effect that small changes can have on a GCM, a nonlinear system.

4. Surface fluxes, low-level atmospheric fields, and air–sea feedback

The sensible and latent heat flux equations, given in section 2d of Part I, depend on the product of variables; therefore, flux anomalies are influenced by both mean (−) and anomalous (′) conditions; for example,

$$Q'_{sh} \sim U'(\overline{T_o - T_a}) + \bar{U}(T_o - T_a)' + U'(T_o - T_a)' - \overline{U'(T_o - T_a)'}, \quad (1)$$

where Q_{sh} is the sensible heat flux, U the wind speed, T_o the ocean surface temperature, and T_a the air temperature. (The drag coefficient used to compute Q_{sh} is a constant in the CCM0A.) The TP anomalies are obtained from the difference between the UNEL and UNCL simulations, where the UNCL values represent mean conditions; with this construct $\overline{U'(T_o - T_a)'}$ is defined to be zero in (1). In the following analysis we focus on the near-surface wind and temperature fields and their relationship to the surface sensible heat flux anomalies; the formation of T_o anomalies and their influence on the surface fluxes in the North Pacific is discussed in MAA and Part I.

The climatological wind and temperature fields at the lowest model level ($\sigma = 0.991$, approximately 100 m above the surface) are shown over the North Pacific in Figs. 3a and 3b. Cyclonic circulation associated with the Aleutian Low is centered at 55°N, 175°W. To the south of the low, strong westerlies are located between 35°N and 50°N, and the winds have a northward component that is greatest in the vicinity of the date line. Weak winds ($\bar{U} < 2$ m s^{-1}) associated with the subtropical high extend across much of the Pacific at 30°N, and the northeast trades are found along the southern edge of the domain. Off the Asian coast, northwesterly winds advect cold continental air over the Pacific; as a result, the isotherms are aligned from the southwest to the northeast in the western half of the basin but become more zonal to the east of the date line. The temperature gradient is strongest in the northwest Pacific and decreases to the south and east.

Comparing Figs. 3a and 3b with observations from the Comprehensive Ocean–Atmosphere Data Set (COADS) indicates that the wind direction in the CCM is realistic over most of the domain but the strong northward component in the central Pacific is absent in the data. The model's wind speed is about 25% greater than observed while the surface air temperature is roughly 10°C too cold in the northwest Pacific. The over (under) estimation of $U(T_a)$ in the CCM0A primarily results from using unmodified values at the lowest sigma level to represent conditions at 10 m above the surface (Graham et al. 1989).

The anomalous TP (UNEL-UNCL) wind speed (U') and direction (v) are shown in Fig. 3c. (Recall that the SSTs in the North Pacific are prescribed in these simulations.) The wind vectors suggest a southeastward displacement of the cyclonic circulation, consistent with the negative SLP anomaly in the central Pacific (Fig. 2a). The resulting southward shift of the westerlies causes decreased wind speeds across most of the Pacific north of 45°N and increased wind speeds between 30°N and 45°N to the west of 140°W. The maximum absolute values of U' are found in the central Pacific. The northward wind anomalies located in the eastern part of the basin are strongest at 45°N, 150°W.

An analysis of the near-surface thermal budget indicates that the TP air temperature anomalies in Fig. 3d are primarily caused by advection and vertical mixing. In the west Pacific, the southward shift of the advection of cold Asian air results in negative (positive) temperature anomalies south (north) of 45°N, while in the east Pacific, anomalously warm air is associated with southerly wind anomalies. The magnitude of T'_a is greatest over Alaska and Siberia where the limited surface heat capacity is unable to buffer anomalous temperature advection associated with strong land–ocean thermal contrasts. Over the ocean, the T_a anomalies caused by advection are partially compensated by changes in Q_{sh}. For example, the enhanced advection of cold air to the east of Japan results in $U' > 0$ and $T'_a < 0$, which increases the upward flux of heat from the ocean. Convective adjustment and vertical diffusion then mix the heat within the lowest few layers of the CCM. In the central Pacific (~35°N, 180°), where the anomalous temperature advection is weak, T'_a is negative due to the mixing of cold air down to the surface and a small amount of additional cooling by longwave radiation and adiabatic adjustment.

Both the wind speed and air temperature contribute to the TP sensible heat flux anomalies over the North Pacific. Weaker winds and warmer air temperatures cause positive flux anomalies into the ocean in the north and east Pacific; the opposite occurs to the west of 165°W between 30°N and 45°N (the TP flux anomalies are shown in Fig. 18 of Part I). An examination of the three terms in (1) indicates that Q'_{sh} is

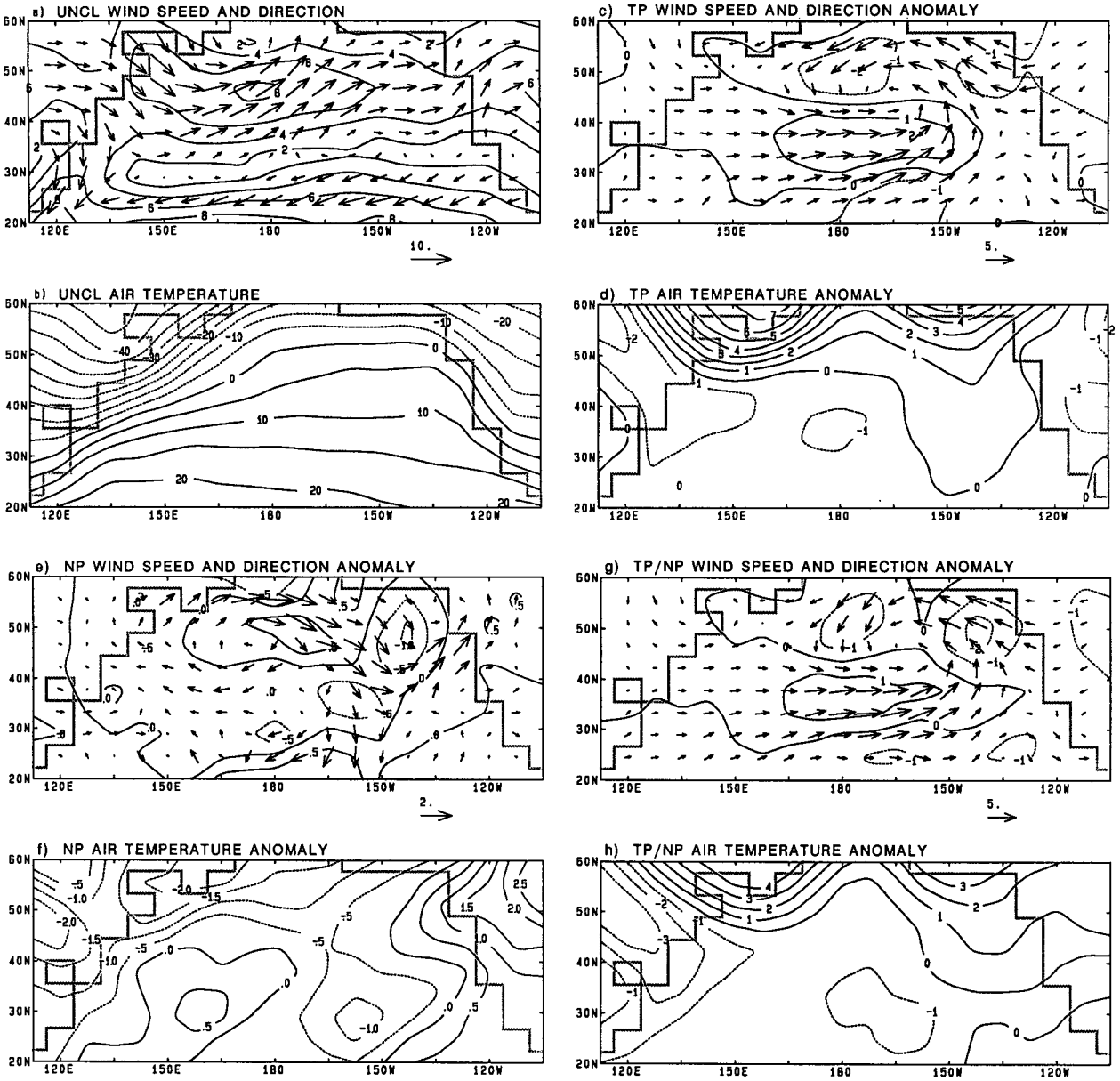

FIG. 3. The winter UNCL (a) wind speed (U) and direction ($\mathbf{v}$) and (b) air temperature (T_a) at the lowest model layer ($\sigma = 0.991$) over the North Pacific. The contour interval is 2 m s^{-1} in (a) and 5°C in (b). The wind and temperature TP, NP, and TP/NP anomaly fields are given in figures (c) and (d), (e) and (f), and (g) and (h), respectively. Note that the contoured values of U' are computed from the daily wind speed differences that are then seasonally averaged, while $\mathbf{V}'$ is obtained from the difference between the seasonally averaged wind vectors. The contour interval for the TP and TP/NP anomaly fields is 1 m s^{-1} for U and 1°C for T_a. The NP contour interval is 0.5 m s^{-1} for U and 0.5°C for T_a.

primarily controlled by $\bar{U}(T_o - T_a)'$ in the east Pacific, $\bar{U}(T_o - T_a)'$ and $U'(T_o - T_a)'$ in the northwest Pacific, and $\bar{U}(T_o - T_a)'$ and $U'(\overline{T_o - T_a})$ west of 160°W between 30° and 45°N. Time filtering Q_o' (see Alexander 1990b) indicates that the surface forcing associated with storms and planetary-scale waves are of comparable strength, but the storm-scale forcing is slightly larger in the west Pacific while the planetary-scale forcing is larger in the far North Pacific.

The NP wind and temperature anomalies are shown in Figs. 3e and 3f. Recall that NP anomalies, obtained from the difference between the COEL and UNEL simulations, indicate the modification of the atmospheric response to tropical forcing due to air–sea feedback in the North Pacific. The anomalies in the atmospheric fields associated with the North Pacific SST anomalies are generally smaller and not as coherent as those due solely to the prescribed tropical SST anom-

alies. Air–sea feedback is associated with cyclonic circulation centered at 52°N, 135°W (Fig. 3e), approximately 10° downstream of the maximum warm SST anomaly in the northeast Pacific. Anticyclonic circulation centered at 48°N, 175°E is located to the north of the cold SST anomaly. The NP wind anomalies, which generally oppose the TP anomalies, are easterly over the north-central Pacific and northerly between 145°W and 170°W over the entire meridional extent of the domain. Negative U' values (where primes now denote NP anomalies) are found in the northeast Pacific and positive values in the north central Pacific.

A detailed heat budget of the lowest CCM layers indicates that the anomalous NP heating/cooling caused by Q'_{sh} is primarily compensated by temperature advection, convective adjustment, and vertical diffusion. If the surface heat exchange were the only process operating, then the air temperature would adjust to the underlying SST anomalies, and the T'_a pattern in Fig. 3f would match the North Pacific SST anomaly pattern shown in Fig. 1. Anomalously warm air overlies warm SST anomalies in the vicinity of 25°N, 150°E and along the west coast of North America, and cold air is found above the cold SST anomalies between 140°W and 160°W at around 30°N. However, the fields have different signs over more than half of the domain, indicating that T'_a cannot be explained by adjustment alone. The low air temperatures between 150°W and 170°W coincide with anomalous cold-air advection by northerly winds. In the northwest corner of the domain, negative T'_a values are associated with anomalous westerlies that transport cold air from Asia. In general, the NP T_a anomalies (Fig. 3f) are opposite to the TP anomalies (Fig. 3d), indicating that air–sea feedback in the North Pacific is acting to damp the atmospheric response to tropical SST anomalies.

The TP/NP wind and temperature anomalies are shown in Figs. 3g and 3h, respectively. When the effects of the tropical and midlatitude SST anomalies are considered together, the anomalous cyclonic circulation becomes more concentric and shifts slightly eastward compared with the response to tropical SST anomalies (Fig. 3c). The magnitudes of the TP/NP negative temperature anomalies are larger in the far west and south-central Pacific, and the positive anomalies are smaller in the northern part of the domain when contrasted with the TP anomalies.

The anomalous NP net surface energy flux (Q'_0) is shown in Fig. 4, where positive values indicate upward flux anomalies. The NP surface flux and SST anomaly patterns generally resemble each other, suggesting a negative feedback between Q'_0 and SST′ (Cayan 1990, Part I) since heat is removed (added) where the mixed layer is anomalously warm (cold). The influence of NP T'_a and U' on the flux field is also apparent. For example, at 50°N, 140°W positive surface flux anomalies are found above warm SST anomalies, but decreased wind speed and increased surface air temperature (Figs. 3e and 3f) limit the magnitude of Q'_0. Positive air–sea feedback occurs in a small area near 45°N, 125°W where the SST and flux anomalies have opposite signs.

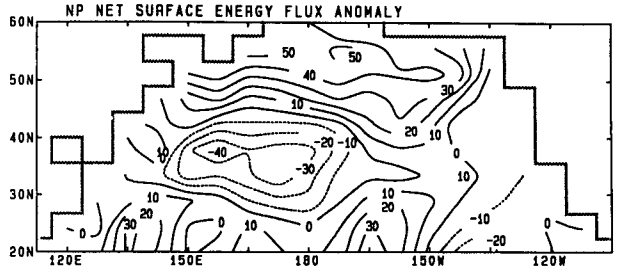

FIG. 4. NP surface energy flux anomaly field during winter (contour interval is 10 W m^{-2}). Positive values denote anomalous upward fluxes.

5. Atmospheric anomalies associated with North Pacific SSTs

The NP surface energy flux anomalies are associated with changes in the Northern Hemisphere SLP, geopotential height, and precipitation fields. However, these changes vary widely among the individual cases; therefore, we will limit our discussion of features in the composite fields to those that are prevalent in the individual cases. The composite NP SLP and 700-mb and 200-mb height anomaly fields are shown in Fig. 5. The similarity of the patterns at the three levels indicates that the NP anomalies are approximately equivalent barotropic. The anomalies have an equivalent barotropic structure over most of the Northern Hemisphere in all five cases, but due to one case, the composite includes negative SLP anomalies beneath positive geopotential height anomalies over central Canada. The magnitude of the composite NP anomaly centers range between 2.5 and 4 mb at the surface and 20 to 65 m at upper levels.

Comparing Fig. 5 with Fig. 2 indicates that the SLP and geopotential anomalies associated with the North Pacific SST anomalies have a similar pattern but opposite sign as the atmospheric response to the prescribed tropical SST anomalies. Air–sea feedback in the North Pacific acts to damp the response to the TP SST anomalies in four of the five cases. The NP anomalies are approximately 25% to 40% as large as the TP anomalies, which is roughly the same as the ratio of the NP to the TP SST anomalies (Fig. 1). The TP/NP anomaly fields (not shown) are equivalent to adding the corresponding fields in Figs. 2 and 5. As a result of air–sea feedback in the North Pacific, the composite TP/NP anomaly centers near the date line are reduced and shifted eastward compared with the TP fields. The TP/NP fields are in better agreement with the magnitude and patterns of the observed anomalies associated with El Niño (van Loon and Madden 1981; van

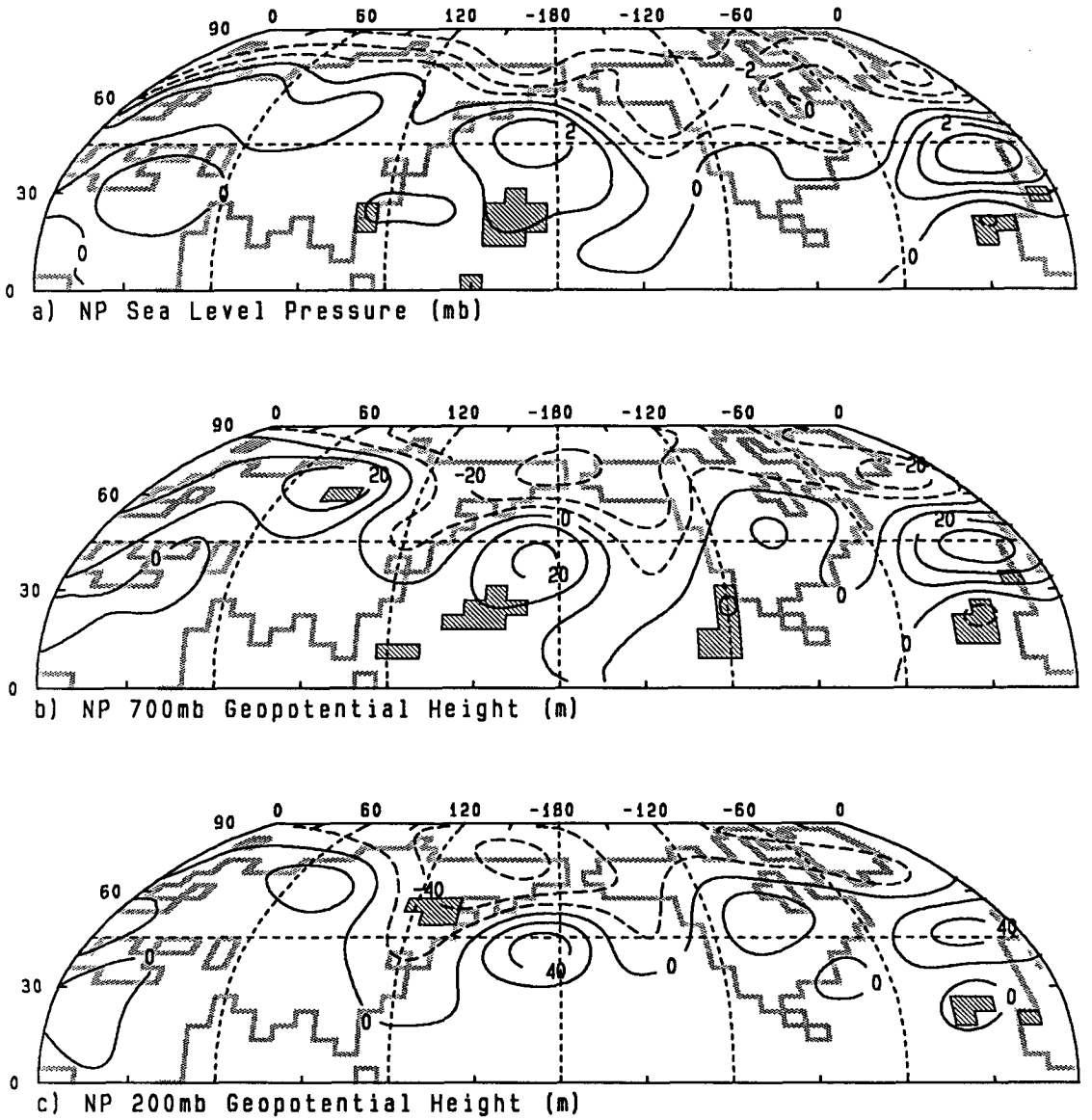

FIG. 5. The winter NP anomaly fields of (a) SLP, (b) 700-mb height, and (c) 200-mb height. The contour intervals in (a), (b), and (c) are 1 mb, 10 m, and 20 m, respectively. Grid squares where the t statistic is significant at the 5% level are shaded.

Loon and Rogers 1981; Mo and Livezey 1986) than the response to tropical anomalies alone. However, the influence of air–sea feedback in the North Pacific on the anomaly patterns is uncertain due to the large intersample variability, as discussed in the following paragraphs.

The NP SLP t-statistic values (Fig. 5a) are significant at the 5% level over a small region in the central Pacific and at a few other grid points in the subtropics. At 700 and 200 mb, the NP anomaly centers do not contain grid squares with significant t values. The relatively low number of significant grid squares indicates that the magnitude of the anomalies is small with respect to the variability of the anomaly pattern. The difficulty of detecting changes associated with realistic ($\leq |2°C|$) midlatitude SST anomalies above the internal variability in a GCM was also noted by Palmer and Sun (1985).

The variability of the individual NP samples is readily apparent from the five 200-mb geopotential height anomaly fields (Fig. 6) that are used to construct the ensemble average (Fig. 5c). Only the first field resembles the composite, and the five cases are distinctly different from each other. The first NP field includes alternating positive and negative geopotential anomalies along 45°N. The anomalies in fields 2 and 4 are elongated in the zonal direction with negative geopotential anomalies at high latitudes, positive anomalies

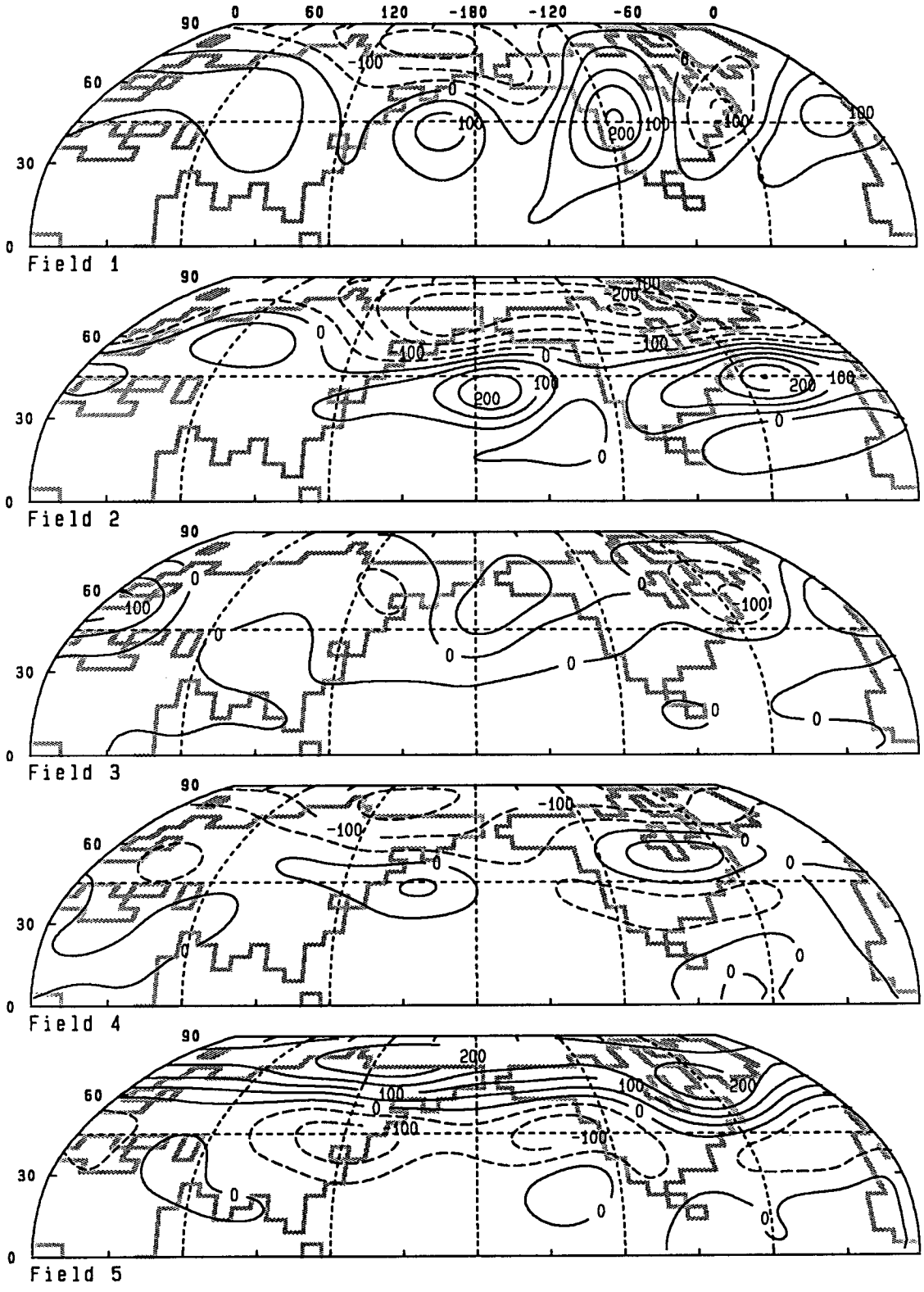

FIG. 6. Five realizations of the winter NP 200-mb height anomaly field (contour interval is 50 m).

at midlatitudes, and weaker negative anomalies in the subtropics. Field 5 also shows a zonal structure but the bands are opposite in sign to those in field 2. The strongest feature in field 3 is an east–west dipole with a trough over the Labrador Sea and a ridge over western Europe. While there are differences between the North Pacific SST anomalies in the five samples, the amount of variability is not nearly as large as in the NP atmospheric anomaly fields; that is, all five SST anomaly fields have cold water in the central Pacific and warm water in the northeast Pacific and off the coast of Mexico.

Figure 7 shows the ensemble NP precipitation anomaly field superimposed on the simulated Pacific storm tracks in the UNEL composite. The storm tracks were sketched from precipitation maxima, roughly where the daily precipitation rate exceeded 4 mm d^{-1} when averaged over the winter season. Palmer and Sun (1985) and Lau and Nath (1990) also used precipitation anomalies to identify changes in the oceanic storm tracks due to midlatitude SST anomalies. Comparing the NP precipitation anomalies to the UNEL composite indicates how air–sea feedback in the North Pacific alone may influence the position and strength of activity making up the storm tracks.

The NP precipitation anomalies over the North Pacific may be partially related to the local SST anomalies. Precipitation is reduced by over 1.0 mm d^{-1} above the cold NP SST anomaly in the central Pacific. There is also a reduction in the net surface energy flux (Fig. 4) and evaporation upstream from the negative precipitation anomaly, which would reduce the oceanic input of energy and moisture available for the development and maintenance of storms. The decrease in precipitation suggests that local air–sea feedback may cause a weakening of activity in the southern branch of the Pacific storm track (Fig. 7). While the reduction in precipitation in the central Pacific is significant at the 5% level and appears in all five cases, a local anomaly may still be a chance occurrence, as we have not tested the significance of the entire field.

The NP SST and precipitation anomalies do not always vary in unison; for example, precipitation is reduced above the warm SSTs in the Gulf of Alaska. In this region, decreased precipitation is associated with anomalous subsidence, low-level divergence, and northwesterly winds (Fig. 3e). The latter reduces the advection of moisture into the storm-track axis that passes just to the south of Alaska.

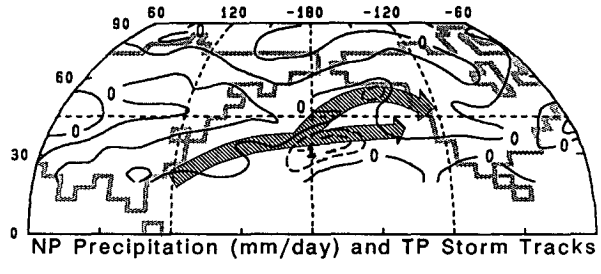

FIG. 7. The winter NP precipitation anomaly field (contour interval is 0.5 mm d^{-1}). Storm tracks, indicated by the wide stippled arrow, are derived by tracing the maximum precipitation values (which generally exceed 4 mm d^{-1}) in the UNEL composite.

6. Summary and conclusions

Using a series of model simulations, we examined the influence of air–sea interaction in the North Pacific during El Niño on the formation of atmospheric anomalies. As a first step, we analyzed the atmospheric changes due solely to prescribed El Niño SST anomalies in the tropical Pacific, focusing on the near-surface fields over the North Pacific during winter. The wind and temperature anomalies and surface flux anomalies were related to a southeastward shift and deepening of the Aleutian Low. The wind-speed anomalies were greatest in the central Pacific; westerlies were reduced (enhanced) to the north (south) of the zonally elongated low-pressure anomaly centered at 45°N. Enhanced wind speeds to the south of the anomalous low and the associated advection of cold continental air result in lower air temperatures to the east of Japan, while anomalous southerly winds advect warm air over the northeast Pacific. As a result, the downward surface heat flux anomalies are positive (negative) in the northeast (central) Pacific.

The SST and atmospheric anomalies that result from midlatitude air–sea interaction (with El Niño conditions still prescribed in the tropical Pacific) were obtained from the difference between two sets, each containing five simulations: in one set the CCM was coupled to a mixed-layer model in the North Pacific while in the second set climatological SSTs were prescribed in the North Pacific. The simulated North Pacific SST anomalies resulted in regional changes in temperature, wind, and precipitation. The near-surface air temperature anomalies primarily reflected the effects of advection, local adjustment to the SST anomalies, and the heat transfer by convective adjustment and vertical diffusion. A reduction in precipitation, which occurred above the cold SST anomaly in the central Pacific, suggested a possible decrease of activity in the Pacific storm track in the vicinity of the date line. While this local decrease in precipitation was significant, it may still have been a chance occurrence, as the field significance was not tested.

The simulated North Pacific SST anomalies and the resulting Northern Hemisphere atmospheric geopotential height anomalies were roughly one-third as large as those due solely to prescribed El Niño conditions in the tropical Pacific. The atmospheric response to the tropical SST anomalies featured a zonally banded structure with maxima in the Pacific and Atlantic sectors. Including air–sea feedback in the North Pacific

damped the tropically induced anomalies in four out of the five cases.

While the North Pacific SST anomalies clearly reflected the atmospheric forcing associated with El Niño conditions in the tropical Pacific (Part I), the influence of the midlatitude SST anomalies on the large-scale atmospheric circulation was much more ambiguous. The changes in the SLP and geopotential height associated with the North Pacific SST anomalies were statistically significant at only a few grid points over the entire Northern Hemisphere. Large differences between the five independent samples used to construct the ensemble average indicated that if a consistent signal was present it was obscured by noise.

The anomaly patterns and the amount of intersample variability found in our experiment differ from that of Pitcher et al. (1988) even though both studies examined the adjustment of the CCM0A to comparable North Pacific SST anomaly fields. For example, the positive anomaly over the west Pacific in our simulations does not appear in their study, and they obtained statistically significant anomalies in the PNA region, in contrast to our results. Several factors may contribute to these differences. 1) The SST anomalies used by Pitcher et al. were larger and had a somewhat different configuration than those that formed in the mixed-layer ocean model. The GCM experiments of Palmer and Sun (1985) suggest that if larger SST anomalies had formed in the North Pacific Ocean model the atmospheric response would likely be larger and possibly more consistent. In addition, the dominant atmospheric teleconnection patterns are sensitive to the exact location of the midlatitude SST anomalies (Namias 1972; Wallace and Jiang 1987; Lau and Nath 1990). 2) Air–sea feedback, included in our study, may act to enhance or damp certain modes or scales of motion (Frankignoul 1985b). Our study supports the findings of Hendon and Hartmann (1982) in that midlatitude air–sea feedback suppressed the extratropical atmospheric anomalies associated with tropical heating. 3) The anomalies in our study were defined with respect to a background state that included strong tropical forcing. Linear models suggest that the evolution of atmospheric anomalies is very sensitive to the background state. 4) The simulations in this study were performed using the seasonal-cycle version of the CCM, while Pitcher et al. used perpetual January simulations. Anomalies are likely to be more variable and have a different evolution when the model climate evolves with the seasons. 5) Independent sets of GCM simulations are likely to show some differences as a result of internal variability.

Pitcher et al. also performed CCM0A simulations with the reverse SST anomaly pattern specified in the North Pacific, warm (cold) water in the central (east) Pacific. The CCM response to opposite SST anomaly fields was surprisingly similar, indicating that model deficiencies may selectively influence the results or that the atmospheric response to midlatitude SST anomalies is highly nonlinear.

In some regards, the atmospheric anomalies associated with midlatitude air–sea interaction are similar to the results of several modeling studies utilizing realistic prescribed SSTs (Palmer and Sun 1985; Pitcher et al. 1988; Lau and Nath 1990) in that the geopotential anomalies are equivalent barotropic, increase with height in the troposphere, and have an ensemble-averaged amplitude of about 30–50 m per 1°C SST anomaly at the 500-mb level. However, in contrast with our results, Wallace and Jiang (1987) and Lau and Nath (1990) found that midlatitude atmospheric anomalies are more closely associated with midlatitude than with tropical SST anomalies. This study examines only the anomalies that develop under El Niño conditions, where the prescribed tropical SST anomalies are large (twice the El Niño composite of Rasmusson and Carpenter 1982) and have the same evolution in all of the experiments. The observed midlatitude atmospheric circulation and North Pacific SST fields exhibit considerable variability among the different El Niño events. Wallace et al. (1990) found that the first EOF of December–February SSTs in the North Pacific exhibits a modest temporal correlation (−0.54) with an index of SSTs in the equatorial Pacific. The results from Wallace and Jiang, Wallace et al., and Lau and Nath suggest that midlatitude processes not associated with El Niño strongly contribute to the connection between atmospheric and oceanic anomaly patterns in the Northern Hemisphere.

Acknowledgments. This work comprised part of my Ph.D. research at the University of Wisconsin. I wish to thank John Kutzbach, my Ph.D. advisor, for his support and guidance. Robert Chervin of the National Center for Atmospheric Research (NCAR) provided model history tapes and a multitasked version of the Community Climate Model. Rich Selin and Pat Behling helped to draft the figures. The scientific input and comments from David Battisti, Martin Hoerling, and Klaus Weickmann are greatly appreciated. Arthur Miller, Robert Livezey, and an anonymous reviewer suggested several improvements to the manuscript.

This research project was supported under Grant ATM89-02849 from the National Science Foundation's Climate Dynamics program to the University of Wisconsin–Madison. Additional support for the author and part of the publication costs were provided by a CIRES fellowship at the University of Colorado. The computations were made at NCAR, which is sponsored by the National Science Foundation, with Grant 35381044 from the NCAR Scientific Computing Division.

REFERENCES

Alexander, M. A., 1990a: Simulation of the response of the North Pacific Ocean to the anomalous atmospheric circulation associated with El Niño. *Climate Dyn.*, **5**, 53–65.

——, 1990b: Interactions between the North Pacific Ocean and the Northern Hemisphere Atmosphere During El Niño. Ph.D. Thesis, University of Wisconsin, Madison, 150 pp.
——, 1992: Midlatitude air–sea interaction during El Niño. Part I: the North Pacific Ocean. *J. Climate,* **5,** 944–958.
Alexander, R. C., and R. L. Mobley, 1976: Monthly average sea-surface temperature and ice-pack limits in a 1° global grid. *Mon. Wea. Rev.,* **104,** 143–148.
Aragão, J. O. R., 1986: A general circulation model investigation of the atmospheric response to El Niño. Cooperative thesis No. 100, University of Miami and National Center for Atmospheric Research, 144 pp.
Bjerknes, J., 1964: Atlantic air–sea interaction. *Advances in Geophysics,* No. 20, Academic Press, 1–82.
——, 1969: Atmospheric teleconnections from the equatorial Pacific. *Mon. Wea. Rev.,* **97,** 163–172.
Blackmon, M. L., J. E. Geisler, and E. J. Pitcher, 1983: A general circulation model study of January climate anomaly patterns associated with interannual variation of equatorial Pacific sea surface temperatures. *J. Atmos. Sci.,* **40,** 1410–1425.
Cayan, D. R., 1990: Variability of latent and sensible heat flux over the oceans. Ph.D. dissertation, University of California, San Diego, 199 pp.
Chervin, R. M., 1986: Interannual variability and seasonal climate predictability. *J. Atmos. Sci.,* **43,** 233–251.
——, and S. H. Schneider, 1976: On determining the statistical significance of climate experiments with general circulation models. *J. Atmos. Sci.,* **33,** 405–412.
——, W. M. Washington, and S. H. Schneider, 1976: Testing the statistical significance of the response of the NCAR general circulation model to North Pacific Ocean surface temperature anomalies. *J. Atmos. Sci.,* **33,** 413–423.
——, J. E. Kutzbach, D. D. Houghton, and R. G. Gallimore, 1980: Response of the NCAR general circulation model to prescribed changes in ocean surface temperature. Part II: Midlatitude and subtropical changes. *J. Atmos. Sci.,* **37,** 308–332.
Davis, R. E., 1976: Predictability of sea surface temperature and sea level pressure anomalies over the North Pacific Ocean. *J. Phys. Oceanogr.,* **6,** 249–266.
——, 1978: Predictability of sea level pressure anomalies over the North Pacific Ocean. *J. Phys. Oceanogr.,* **8,** 233–246.
Frankignoul, C., 1985a: Multivariate analysis of sensitivity studies with atmospheric GCM's. *Coupled Atmosphere–Ocean Models,* Elsevier Oceanogr. Ser., Vol. 40, J. C. J. Nihoul, Ed., Elsevier, 199–209.
——, 1985b: Sea surface temperature anomalies, planetary waves, and air–sea feedback in the middle latitudes. *Rev. Geophys.,* **23,** 357–390.
——, and K. Hasselmann, 1977: Stochastic climate models. Part 2: Application to sea-surface temperature anomalies and thermocline variability. *Tellus,* **29,** 284–305.
——, and R. W. Reynolds, 1983: Testing a dynamical model for midlatitude sea surface temperature anomalies. *J. Phys. Oceanogr.,* **13,** 1131–1145.
——, and A. Molin, 1988a: Response of the GISS general circulation model to a midlatitude sea surface temperature anomaly in the North Pacific. *J. Atmos. Sci.,* **45,** 95–108.
——, and ——, 1988b: Analysis of the GISS GCM response to a sea surface temperature anomaly using a linear model. *J. Atmos. Sci.,* **45,** 3833–3845.
Graham, N. E., T. P. Barnett, R. M. Chervin, M. E. Schlessinger, and U. Schlese, 1989: Comparisons of GCM and observed surface wind fields over the tropical Indian and Pacific Oceans. *J. Atmos. Sci.,* **46,** 760–788.
Geisler, J. E., M. L. Blackmon, G. T. Bates, and S. Muñoz, 1985: Sensitivity of January climate response to the magnitude and position of equatorial Pacific sea-surface temperature anomalies. *J. Atmos. Sci.,* **42,** 1047–1049.
Hannoschöck, G., and C. Frankignoul, 1985: Multivariate statistical analysis of a sea surface temperature anomaly experiment with the GISS general circulation model 1. *J. Atmos. Sci.,* **42,** 1430–1450.
Harnack, R. P., 1979: A further assessment of winter temperature predictions using objective methods. *Mon. Wea. Rev.,* **107,** 250–267.
——, 1982: Objective winter temperature forecasts: An update and extension to the western United States. *Mon. Wea. Rev.,* **110,** 287–295.
Haworth, C., 1978: Some relationships between sea surface temperature anomalies and surface pressure anomalies. *Quart. J. Roy. Meteor. Soc.,* **104,** 131–146.
Heald, R. C., and J.-W. Kim, 1979: Parameterization of the oceanic mixed layer for use in general circulation models. Department of Atmospheric Science and Climatic Research Institute, Oregon State University, Corvalis, Rep. No. 10, 48 pp.
Hendon, H. H., and D. L. Hartmann, 1982: Stationary waves on a sphere: Sensitivity to thermal feedback. *J. Atmos. Sci.,* **39,** 1906–1920.
Holopainen, E. O., 1983: Transient eddies in mid-latitudes: observations and interpretation. *Large-Scale Dynamical Processes in the Atmosphere,* B. J. Hoskins and R. P. Pearce, Eds., Academic Press, 201–233.
Hoerling, M. P., T. K. Schaack, and D. R. Johnson, 1990: Heating distributions from January and July simulations of NCAR Community Climate Models. *J. Climate,* **3,** 417–434.
Horel, J. D., and J. M. Wallace, 1981: Planetary-scale atmospheric phenomena associated with the Southern Oscillation. *Mon. Wea. Rev.,* **109,** 813–829.
Hoskins, B. J., and D. J. Karoly, 1981: The steady linear response of a spherical atmosphere to thermal and orographic forcing. *J. Atmos. Sci.,* **38,** 1179–1196.
Houghton, D. D., J. E. Kutzbach, M. McClintock, and D. Suchman, 1974: Response of a general circulation model to a sea temperature perturbation. *J. Atmos. Sci.,* **31,** 857–868.
Kang, I.-S., and N.-C. Lau, 1986: Principal modes of atmospheric variability in model atmospheres with and without anomalous sea surface temperature forcing in the tropical Pacific. *J. Atmos. Sci.,* **43,** 2719–2735.
Keshavamurty, R. N., 1982: Response of the atmosphere to sea surface temperature anomalies over the equatorial Pacific and the teleconnections of the Southern Oscillation. *J. Atmos. Sci.,* **39,** 1241–1259.
Kutzbach, J. E., R. M. Chervin, and D. D. Houghton, 1977: Response of the NCAR general circulation model to prescribed changes in ocean surface temperature, Part I: Midlatitude changes. *J. Atmos. Sci.,* **34,** 1200–1213.
Lau, N.-C., 1988: Variability of the observed midlatitude storm tracks in relation to low-frequency changes in the circulation pattern. *J. Atmos. Sci.,* **45,** 2718–2743.
——, and M. J. Nath, 1990: A general circulation model study of the atmospheric response to extratropical SST anomalies observed in 1950–79. *J. Climate,* **3,** 965–989.
Livezey, R. E., and K. C. Mo, 1987: Tropical–extratropical teleconnections during Northern Hemisphere winter. Part II: Relationships between monthly mean Northern Hemisphere circulation patterns and proxies for tropical convection. *Mon. Wea. Rev.,* **115,** 3115–3132.
Malone, R. C., E. J. Pitcher, M. L. Blackmon, K. Puri, and W. Bourke, 1984: The simulation of stationary and transient geopotential height eddies in January and July with a spectral general circulation model. *J. Atmos. Sci.,* **41,** 1394–1419.
Mo, K. C., and R. E. Livezey, 1986: Tropical–extratropical geopotential height teleconnections during Northern Hemisphere winter. *Mon. Wea. Rev.,* **114,** 2488–2515.
Namias, J., 1959: Recent seasonal interactions between North Pacific waters and the overlying atmospheric circulation. *J. Geophys. Res.,* **64,** 631–646.

——, 1964: Seasonal persistence and recurrence of European blocking during 1958–1960. *Tellus,* **3,** 394–407.

——, 1965: Macroscopic association between mean monthly sea surface temperature and the overlying winds. *J. Geophys. Res.,* **70,** 2307–2318.

——, 1969: Seasonal interactions between the North Pacific Ocean and the atmosphere during the 1960's. *Mon. Wea. Rev.,* **97,** 173–192.

——, 1972: Experiments in objectively predicting some atmospheric and oceanic variables for the winter of 1971–1972. *J. Appl. Meteor.,* **11,** 1164–1174.

——, 1976: Some statistical and synoptic characteristics associated with El Niño. *J. Phys. Oceanogr.,* **6,** 130–138.

Niiler, P. P., and E. B. Kraus, 1977: One-dimensional models of the upper ocean. *Modeling and Prediction of the Upper Layers of the Ocean,* E. B. Kraus, Ed., Pergamon Press, 143–172.

Palmer, T. N., and Z. Sun, 1985: A modelling and observational study of the relationship between sea surface temperature in the north-west Atlantic and the atmospheric general circulation. *Quart. J. Roy. Meteor. Soc.,* **111,** 947–975.

Pan, Y. H., and A. H. Oort, 1983: Global climate variations connected with sea surface temperature anomalies in the eastern equatorial Pacific Ocean for the 1958–73 period. *Mon. Wea. Rev.,* **111,** 1244–1258.

Pitcher, E. J., R. C. Malone, V. Ramanathan, M. L. Blackmon, K. Puri, and W. Bourke, 1983: January and July simulations with a spectral general circulation model. *J. Atmos. Sci.,* **40,** 580–604.

——, M. L. Blackmon, G. T. Bates, and S. Muñoz, 1988: The effects of North Pacific sea surface temperature anomalies on the January climate of a general circulation model. *J. Atmos. Sci.,* **45,** 173–188.

Pollard, R. T., R. C. Millard, 1970: Comparison between observed and simulated wind-generated inertial oscillations. *Deep-Sea Res.,* **17,** 813–821.

Ramanathan, V., E. J. Pitcher, R. C. Malone, and M. L. Blackmon, 1983: The response of a spectral general circulation model to refinements in radiative processes. *J. Atmos. Sci.,* **40,** 605–630.

Rasmusson, E. M., and T. H. Carpenter, 1982: Variations in tropical sea surface temperature and surface wind fields associated with the Southern Oscillation/El Niño. *Mon. Wea. Rev.,* **110,** 354–384.

Ratcliffe, R. A. S., and R. Murray, 1970: New lag associations between North Atlantic sea temperature and European pressure applied to long-range weather forecasting. *Quart. J. Roy. Meteor. Soc.,* **96,** 226–246.

Salmon, R., and M. C. Hendershott, 1976: Large-scale air-sea interactions with a simple general circulation model. *Tellus,* **28,** 228–242.

Sardeshmukh, P. D., and B. J. Hoskins, 1988: The generation of global rotational flow by steady, idealized tropical divergence. *J. Atmos. Sci.,* **45,** 1228–1251.

Semtner, A. J., 1984: Development of efficient, dynamical ocean–atmosphere models for climatic studies. *J. Climate. Appl. Meteor.,* **23,** 353–374.

Shukla, J., and B. Bangaru, 1979: Effect of a Pacific sea surface temperature anomaly on the circulation over North America: A numerical experiment with the GLAS model. Report of the JOC study conference on climate models: Performance, intercomparison and sensitivity studies, WMO, 1, 501–518.

——, and J. M. Wallace, 1983: Numerical simulation of the atmospheric response to equatorial Pacific sea-surface temperature anomalies. *J. Atmos. Sci.,* **40,** 1613–1630.

Simmons, A. J., J. M. Wallace, and G. W. Branstator, 1983: Barotropic wave propagation and instability, and atmospheric teleconnection patterns. *J. Atmos. Sci.,* **40,** 1363–1392.

Spar, J., 1973: Some effects of surface anomalies in a global circulation model. *Mon. Wea. Rev.,* **101,** 91–100.

van Loon, H., and R. A. Madden, 1981: The Southern Oscillation. Part I: Global associations with pressure and temperature in northern winter. *Mon. Wea. Rev.,* **109,** 1150–1162.

——, and J. C. Rogers, 1981: The Southern Oscillation. Part II: Associations with changes in the middle troposphere in the northern winter. *Mon. Wea. Rev.,* **109,** 1163–1168.

Wallace, J. M., and D. S. Gutzler, 1981: Teleconnections in the geopotential height field during the Northern Hemisphere winter. *Mon. Wea. Rev.,* **109,** 784–812.

——, and Q. Jiang, 1987: On the observed structure of the interannual variability of the atmosphere/ocean climate system. *Atmospheric and Oceanic Variability,* H. Cattle, Ed., Roy. Meteor. Soc., 17–43.

——, C. Smith, and Q. Jiang, 1990: Spatial patterns of atmosphere–ocean interaction in the northern winter. *J. Climate,* **3,** 990–998.

Walsh, J. E., and M. B. Richman, 1981: Seasonality in the association between surface temperatures over the United States and the North Pacific Ocean. *Mon. Wea. Rev.,* **109,** 767–783.

Washington, W. M., Ed., 1982: Documentation for the Community Climate Model, CCM: Version 0. National Center for Atmospheric Research, Boulder, Colorado. Unpaginated. [NTIS PB82-194192]

Webster, P. J., 1981: Mechanisms determining the atmospheric response to sea-surface temperature anomalies. *J. Atmos. Sci.,* **38,** 554–571.

——, and H. R. Chang, 1988: Energy accumulation and emanation regions at low latitudes: Impacts of a zonally varying basic state. *J. Atmos. Sci.,* **45,** 803–829.